

Subdiffraction incoherent optical imaging via spatial-mode demultiplexing

Mankei Tsang^{1,2,*}

¹*Department of Electrical and Computer Engineering,
National University of Singapore, 4 Engineering Drive 3, Singapore 117583*

²*Department of Physics, National University of Singapore, 2 Science Drive 3, Singapore 117551*

(Dated: May 18, 2022)

I propose a spatial-mode demultiplexing (SPADE) measurement scheme for the far-field imaging of spatially incoherent optical sources. For any object too small to be resolved by direct imaging under the diffraction limit, I show that SPADE can estimate its second or higher moments much more precisely than direct imaging can fundamentally do in the presence of photon shot noise. Realizable with far-field linear optics and photon counting, SPADE is expected to find applications in both fluorescence microscopy and astronomy.

I. INTRODUCTION

Recent research, initiated by our group [1–7], has shown that far-field linear optical methods can significantly improve the resolution of two equally bright incoherent optical point sources with sub-Rayleigh separations [1–14], overcoming previously established statistical limits [15–18]. The rapid experimental demonstrations [11–14] have heightened the promise of our approach. An open problem, of fundamental interest in optics and monumental importance to astronomy and fluorescence microscopy, is whether these results can be generalized for arbitrary incoherent sources. Here I take a major step towards solving the problem by proposing a generalized spatial-mode demultiplexing (SPADE) measurement scheme and proving its superiority over direct imaging via a statistical analysis.

The use of coherent optical processing to improve the lateral resolution of incoherent imaging has thus far received only modest attention, as prior proposals [12, 19–24] either did not demonstrate any substantial improvement or neglected the important effect of noise. Using quantum optics and parameter estimation theory, here I show that, for any object too small to be resolved by diffraction-limited direct imaging, SPADE can estimate its second or higher moments much more precisely than direct imaging can fundamentally do in the presence of photon shot noise. Given the usefulness of moments in identifying the size and shape of an object [25], the proposed scheme, realizable with far-field linear optics and photon counting, should provide a major boost to incoherent imaging applications that are limited by diffraction and photon shot noise, including not only fluorescence microscopy [26–29] and space-based telescopes [30] but also ground-based telescopes in the near future [31].

II. BACKGROUND FORMALISM

A. Quantum optics

I begin with the quantum formalism established in Ref. [1] to ensure correct physics. The quantum state of thermal light

with M temporal modes and a bandwidth much smaller than the center frequency can be written as $\rho^{\otimes M}$, where $\rho = (1 - \epsilon)\rho_0 + \epsilon\rho_1 + O(\epsilon^2)$, ϵ is the average photon number per mode assumed to be $\ll 1$ [32, 33], $\rho_0 = |\text{vac}\rangle\langle\text{vac}|$ is the vacuum state, ρ_1 is the one-photon state with a density matrix equal to the mutual coherence function, and $O(\epsilon^2)$ denotes second-order terms, which are neglected hereafter. It is standard to assume that the fields from incoherent objects, such as stellar or fluorescent emitters, are spatially uncorrelated at the source [33]. In a diffraction-limited imaging system, the fields then propagate as waves; the Van Cittert-Zernike theorem is the most venerable consequence [33]. At the image plane of a conventional lens-based two-dimensional imaging system in the paraxial regime [33, 34], this implies

$$\begin{aligned}\rho_1 &= \int d^2\mathbf{R} F(\mathbf{R}) |\psi_{\mathbf{R}}\rangle\langle\psi_{\mathbf{R}}|, \\ |\psi_{\mathbf{R}}\rangle &= \int d^2\mathbf{r} \psi(\mathbf{r} - \mathbf{R}) |\mathbf{r}\rangle,\end{aligned}\quad (1)$$

where $\mathbf{R} = (X, Y)$ is the object-plane position vector, $F(\mathbf{R})$ is the source intensity distribution with normalization $\int d^2\mathbf{R} F(\mathbf{R}) = 1$, $|\mathbf{r}\rangle = a^\dagger(\mathbf{r})|\text{vac}\rangle$ is a one-photon position eigenket on the image plane at position $\mathbf{r} = (x, y)$ with $[a(\mathbf{r}), a^\dagger(\mathbf{r}')] = \delta^2(\mathbf{r} - \mathbf{r}')$ [35], and $\psi(\mathbf{r})$ is the field point-spread function (PSF) of the imaging system. Without loss of generality, the image-plane position vector \mathbf{r} has been scaled with respect to the magnification to follow the same scale as \mathbf{R} [34]. For convenience, I also normalize the position vectors with respect to the width of the PSF to make them dimensionless.

Consider the processing and measurement of the image-plane field by linear optics and photon counting. The counting distribution for each ρ can be expressed as $\langle n_0, n_1, \dots | \rho | n_0, n_1, \dots \rangle$, where $|n_0, n_1, \dots\rangle = (\prod_{j=0}^{\infty} b_j^{\dagger n_j} / \sqrt{n_j!}) |\text{vac}\rangle$, $b_j \equiv \int d^2\mathbf{r} \phi_j^*(\mathbf{r}) a(\mathbf{r})$, $\phi_j(\mathbf{r})$ is the optical mode function that is projected to the j th output, and $[b_j, b_k^\dagger] = \int d^2\mathbf{r} \phi_j^*(\mathbf{r}) \phi_k(\mathbf{r}) = \delta_{jk}$. With the negligence of multiphoton coincidences, the relevant projections are $\{|\text{vac}\rangle, |\phi_j\rangle\}$, with $|\phi_j\rangle \equiv |0, \dots, n_j = 1, \dots, 0\rangle = b_j^\dagger |\text{vac}\rangle = \int d^2\mathbf{r} \phi_j(\mathbf{r}) |\mathbf{r}\rangle$. The zero-photon probability becomes $1 - \epsilon$ and the probability of one photon being detected in the j th mode becomes $\epsilon p(j)$,

* mankei@nus.edu.sg

where

$$p(j) \equiv \langle \phi_j | \rho_1 | \phi_j \rangle = \int d^2 \mathbf{R} F(\mathbf{R}) |\langle \phi_j | \psi_{\mathbf{R}} \rangle|^2 \quad (2)$$

is the one-photon distribution. A generalization of the measurement model using the concept of positive operator-valued measures is possible [1, 3] but not needed here.

For example, direct imaging can be idealized as a measurement of the position of each photon, leading to an expected image given by

$$f(\mathbf{r}) \equiv \langle \mathbf{r} | \rho_1 | \mathbf{r} \rangle = \int d^2 \mathbf{R} F(\mathbf{R}) |\psi(\mathbf{r} - \mathbf{R})|^2, \quad (3)$$

which is a basic result in statistical optics [33, 34]. While Eq. (3) suggests that, similar to the coherent-imaging formalism, the PSF acts as a low-pass filter in the spatial frequency domain [34], the effect of more general optical processing according to Eq. (2) is more subtle and offers surprising advantages, as demonstrated by recent work [1–14] and elaborated in this paper.

Over M temporal modes, the probability distribution of photon numbers $m = (m_0, m_1, \dots)$ detected in the respective optical modes becomes

$$P(m) = \sum_L \mathcal{M}(m|L) \mathcal{B}(L), \quad (4)$$

where $\mathcal{B}(L)$ is the binomial distribution for detecting L photons over M trials with single-trial success probability ϵ and $\mathcal{M}(m|L) = \delta_{L, \sum_j m_j} L! \prod_j [p(j)]^{m_j} / m_j!$ is the multinomial distribution of m given L total photons [36]. The average photon number in all modes becomes $N \equiv M\epsilon$. Taking the limit of $\epsilon \rightarrow 0$ while holding N constant, $\mathcal{B}(L)$ becomes Poisson with mean N , and $P(m) \rightarrow \exp(-N) \prod_j [Np(j)]^{m_j} / m_j!$, which is the widely used Poisson model of photon counting for incoherent sources at optical frequencies [3, 17, 26–30, 32].

B. Parameter estimation

The central goal of imaging is to infer unknown properties of the source distribution $F(\mathbf{R})$ from the measurement outcome m . Here I frame it as a parameter estimation problem, defining $\theta = (\theta_1, \theta_2, \dots)$ as a vector of unknown parameters and assuming the source distribution $F(\mathbf{R}|\theta)$ to be a function of θ . Denote an estimator as $\hat{\theta}(m)$ and its error covariance matrix as $\Sigma_{\mu\nu}(\theta) = \sum_m P(m|\theta) [\hat{\theta}_\mu(m) - \theta_\mu] [\hat{\theta}_\nu(m) - \theta_\nu]$. For any unbiased estimator ($\sum_m \hat{\theta}(m) P(m|\theta) = \theta$), the Cramér-Rao bound (CRB) is given by [36, 37]

$$\Sigma_{\mu\mu}(\theta) \geq [J^{-1}(\theta)]_{\mu\mu}, \quad (5)$$

where $J(\theta)$ is the Fisher information matrix. Assuming the model given by Eq. (4) and a known N , it can be shown [3] that

$$J_{\mu\nu}(\theta) = N \sum_j \frac{1}{p(j|\theta)} \frac{\partial p(j|\theta)}{\partial \theta_\mu} \frac{\partial p(j|\theta)}{\partial \theta_\nu}, \quad (6)$$

which is a well known expression [15–17, 27, 29, 32]. For example, the direct-imaging information, given Eq. (3) and the limit $p(j|\theta) \rightarrow d^2 \mathbf{r} f(\mathbf{r}|\theta)$, is

$$J_{\mu\nu}^{(\text{direct})}(\theta) = N \int d^2 \mathbf{r} \frac{1}{f(\mathbf{r}|\theta)} \frac{\partial f(\mathbf{r}|\theta)}{\partial \theta_\mu} \frac{\partial f(\mathbf{r}|\theta)}{\partial \theta_\nu}. \quad (7)$$

For large N , the maximum-likelihood estimator is asymptotically normal with mean θ and covariance $\Sigma(\theta) = J^{-1}(\theta)$, even though it may be biased for finite N [36, 37]. Bayesian and minimax generalizations of the CRB for any biased or unbiased estimator are possible [5, 37] but not considered here as they offer qualitatively similar conclusions. The Fisher information is nowadays regarded as the standard precision measure in incoherent imaging research, especially in fluorescence microscopy [17, 27–29], where photon shot noise is the dominant noise source and a proper statistical analysis is essential.

III. SPATIAL-MODE DEMULTIPLEXING (SPADE)

SPADE is a technique previously proposed for the purpose of superresolving the separation between two incoherent point sources [1, 6, 7, 9, 12–14]. I now ask how SPADE can be generalized for the imaging of an arbitrary source distribution. Consider the transverse-electromagnetic (TEM) basis $\{|\mathbf{q}\rangle; \mathbf{q} = (q_x, q_y) \in \mathbb{N}^2\}$ [38], where

$$|\mathbf{q}\rangle = \int d^2 \mathbf{r} \phi_{\mathbf{q}}(\mathbf{r}) |\mathbf{r}\rangle, \quad (8)$$

$$\phi_{\mathbf{q}}(\mathbf{r}) \equiv \frac{\text{He}_{q_x}(x) \text{He}_{q_y}(y)}{\sqrt{2\pi q_x! q_y!}} \exp\left(-\frac{x^2 + y^2}{4}\right), \quad (9)$$

and He_q is the Hermite polynomial [39, 40]. Assuming a Gaussian PSF given by $\psi(\mathbf{r}) = \phi_{00}(\mathbf{r})$, which is a common assumption in fluorescence microscopy [27, 29], $|\psi_{\mathbf{R}}\rangle$ is a coherent state [41], and the one-photon density matrix in the TEM basis becomes

$$g(\mathbf{q}, \mathbf{q}'|\theta) \equiv \langle \mathbf{q} | \rho_1(\theta) | \mathbf{q}' \rangle \quad (10)$$

$$= C(\mathbf{q}, \mathbf{q}') \int d^2 \mathbf{R} F(\mathbf{R}|\theta) e^{-(X^2 + Y^2)/4} \times X^{q_x + q'_x} Y^{q_y + q'_y}, \quad (11)$$

where

$$C(\mathbf{q}, \mathbf{q}') \equiv \frac{1}{2^{|\mathbf{q} + \mathbf{q}'|_1} \sqrt{\mathbf{q}! \mathbf{q}'!}}, \quad |\mathbf{q}|_1 \equiv q_x + q_y, \quad \mathbf{q}! \equiv q_x! q_y!. \quad (12)$$

To investigate the imaging capability of SPADE measurements, define

$$\Theta_{\boldsymbol{\mu}}(\theta) \equiv \int d^2 \mathbf{R} F(\mathbf{R}|\theta) e^{-(X^2 + Y^2)/4} X^{\mu_x} Y^{\mu_y}, \quad (13)$$

with $\boldsymbol{\mu} = (\mu_x, \mu_y)$, leading to a linear parameterization of g given by

$$g(\mathbf{q}, \mathbf{q}'|\theta) = C(\mathbf{q}, \mathbf{q}') \Theta_{\mathbf{q} + \mathbf{q}'}. \quad (14)$$

Notice that each Θ_{μ} is a moment of the source distribution filtered by a Gaussian. In particular, if the object is much smaller than the PSF width, the Gaussian can be neglected, and Θ_{μ} becomes a moment of the source distribution itself. This subdiffraction regime is of central interest to superresolution imaging and, as shown in Sec. IV, also a regime in which direct imaging performs relatively poorly. Since a distribution is uniquely determined by its moments [42], $F(\mathbf{R}|\theta) \exp[-(X^2 + Y^2)/4]$ and therefore $F(\mathbf{R}|\theta)$ can be reconstructed given the moments, at least in principle. Note also that the object-moment order μ is nontrivially related to the order of the matrix element via $\mu = \mathbf{q} + \mathbf{q}'$, which is a peculiar feature of incoherent imaging.

A measurement in the TEM basis yields

$$p^{(\text{TEM})}(\mathbf{q}|\theta) = C(\mathbf{q}, \mathbf{q})\Theta_{2\mathbf{q}}, \quad (15)$$

which is sensitive only to moments with even μ_X and μ_Y , as also recognized by Yang *et al.* in Ref. [12]. This measurement is realized by demultiplexing the image-plane optical field in terms of the TEM basis via linear optics before photon counting for each mode and can be implemented by many methods, most commonly found in optical communications [1, 6, 14, 43–45]. To access the other moments, consider interferometry between two TEM modes that implements the projections

$$|+\rangle \equiv \frac{1}{\sqrt{2}}(|\mathbf{q}\rangle + |\mathbf{q}'\rangle), \quad |-\rangle \equiv \frac{1}{\sqrt{2}}(|\mathbf{q}\rangle - |\mathbf{q}'\rangle). \quad (16)$$

This two-channel interferometric TEM (iTEM) measurement leads to

$$\begin{aligned} p^{(\mathbf{q}, \mathbf{q}')}(|+\rangle) &= \beta(\mathbf{q}, \mathbf{q}') + C(\mathbf{q}, \mathbf{q}')\Theta_{\mathbf{q}+\mathbf{q}'}, \\ p^{(\mathbf{q}, \mathbf{q}')}(|-\rangle) &= \beta(\mathbf{q}, \mathbf{q}') - C(\mathbf{q}, \mathbf{q}')\Theta_{\mathbf{q}+\mathbf{q}'}, \end{aligned} \quad (17)$$

$$\beta(\mathbf{q}, \mathbf{q}') \equiv \frac{1}{2}[C(\mathbf{q}, \mathbf{q})\Theta_{2\mathbf{q}} + C(\mathbf{q}', \mathbf{q}')\Theta_{2\mathbf{q}'}]. \quad (18)$$

The dependence on $\Theta_{\mathbf{q}+\mathbf{q}'}$ is the main interest here, as it allows one to access any moment parameter.

For multiparameter estimation and general imaging, multiple TEM and iTEM measurements are needed. To be specific, Table I lists a set of schemes that can be used together to estimate all the moment parameters, while Fig. 1 shows a graphical representation of the schemes in the (q_x, q_y) space. Neighboring modes are used in the proposed iTEM schemes because they maximize the Fisher information, as shown later in Sec. IV. The bases in different schemes are incompatible with one another, so the photons have to be rationed among the 7 schemes, by applying the different schemes sequentially through reprogrammable interferometers or spatial-light modulators [14, 43–45] for example.

IV. STATISTICAL ANALYSIS

A. Direct imaging

Although the proposed SPADE method can in principle perform general imaging, its complexity would not be justifiable

Scheme	Projections	q_x	q_y	μ_X	μ_Y
TEM	$ \mathbf{q}\rangle$	\mathbb{N}	\mathbb{N}	even	even
iTEM1	$ \mathbf{q}\rangle \pm \mathbf{q} + (1, 0)\rangle$	even	\mathbb{N}	1, 5, ...	even
iTEM2	$ \mathbf{q}\rangle \pm \mathbf{q} + (0, 1)\rangle$	\mathbb{N}	even	even	1, 5, ...
iTEM3	$ \mathbf{q}\rangle \pm \mathbf{q} + (1, -1)\rangle$	\mathbb{N}	odd	odd	1, 5, ...
iTEM4	$ \mathbf{q}\rangle \pm \mathbf{q} + (1, 0)\rangle$	odd	\mathbb{N}	3, 7, ...	even
iTEM5	$ \mathbf{q}\rangle \pm \mathbf{q} + (0, 1)\rangle$	\mathbb{N}	odd	even	3, 7, ...
iTEM6	$ \mathbf{q}\rangle \pm \mathbf{q} + (1, -1)\rangle$	\mathbb{N}	even	odd	3, 7, ...

TABLE I. A list of measurement schemes, their projections, and the orders $\mu = (\mu_X, \mu_Y)$ of the moment parameters Θ_{μ} to which they are sensitive. The $1/\sqrt{2}$ factor is omitted from the iTEM projections for brevity.

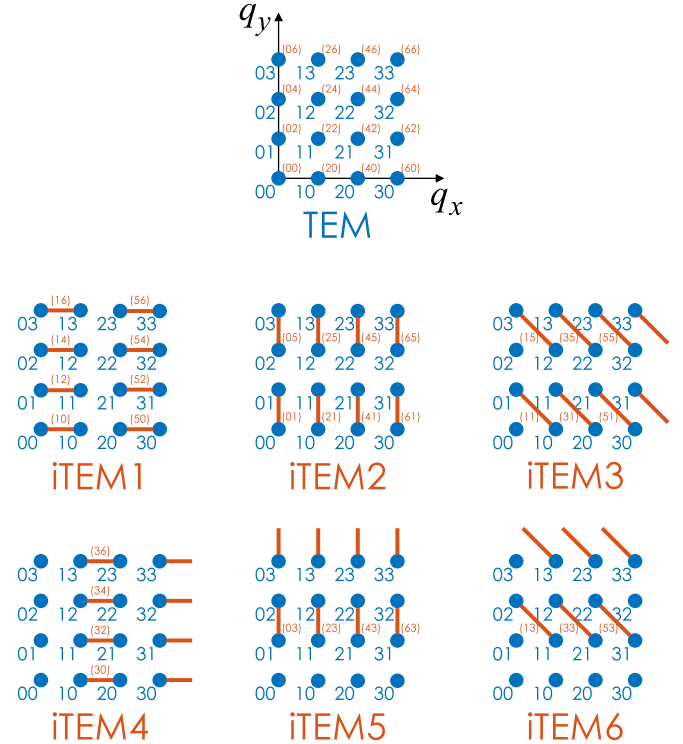


FIG. 1. Each dot corresponds to a TEM mode in the (q_x, q_y) space, and each line connecting two dots denotes an interferometer between two modes in an iTEM scheme. The bracketed numbers are the orders (μ_X, μ_Y) of the moment parameters to which the projections are sensitive. The unconnected dots in some of the iTEM schemes denote the rest of the modes in a complete basis, which can be measured simultaneously to provide extra information.

if it could not offer any significant advantage over direct imaging. To compare their statistical performances, consider first direct imaging with a Gaussian PSF. Expanding $|\psi(\mathbf{r} - \mathbf{R})|^2$ in a Taylor series, I obtain

$$f(\mathbf{r}|\theta) = |\phi_{00}(\mathbf{r})|^2 \left[1 + \sum_{\mu} D_{\mu}(\mathbf{r})\theta_{\mu} \right], \quad (19)$$

$$D_{\mu}(\mathbf{r}) \equiv \frac{\text{He}_{\mu_X}(x) \text{He}_{\mu_Y}(y)}{\mu!}, \quad (20)$$

in terms of the moment parameters defined as

$$\theta_{\boldsymbol{\mu}} \equiv \int d^2 \mathbf{r} F(\mathbf{R}|\theta) X^{\mu_x} Y^{\mu_y}. \quad (21)$$

In terms of this parameterization, the Fisher information becomes

$$J_{\boldsymbol{\mu}\boldsymbol{\nu}}^{(\text{direct})}(\theta) = N \int d^2 \mathbf{r} |\phi_{00}(\mathbf{r})|^2 \frac{D_{\boldsymbol{\mu}}(\mathbf{r}) D_{\boldsymbol{\nu}}(\mathbf{r})}{1 + \sum_{\boldsymbol{\eta}} D_{\boldsymbol{\eta}}(\mathbf{r}) \theta_{\boldsymbol{\eta}}}. \quad (22)$$

Assume now that the support of the source distribution is centered at the origin and has a maximum width Δ much smaller than the PSF width, viz.,

$$\Delta \ll 1, \quad (23)$$

which defines the subdiffraction regime. The parameters are then bounded by $|\theta_{\boldsymbol{\mu}}| \leq (\Delta/2)^{|\boldsymbol{\mu}|_1}$, and the image is so blurred that it resembles the TEM₀₀ mode rather than the object, viz., $f(\mathbf{r}|\theta) = |\phi_{00}(\mathbf{r})|^2 [1 + O(\Delta)]$. Writing the denominator in Eq. (22) as $1 + O(\Delta)$ and applying the orthogonality of Hermite polynomials [39, 40], I obtain

$$J_{\boldsymbol{\mu}\boldsymbol{\nu}}^{(\text{direct})}(\theta) = \frac{N}{\boldsymbol{\mu}!} [\delta_{\boldsymbol{\mu}\boldsymbol{\nu}} + O(\Delta)]. \quad (24)$$

This is a significant result in its own right, as it establishes a fundamental limit to superresolution algorithms for shot-noise-limited direct imaging [19, 46–48], generalizing the earlier results for two sources [15–17] and establishing that, at least for a Gaussian PSF, the moments are a natural, approximately orthogonal [49] set of parameters for subdiffraction objects.

B. SPADE

To investigate the performance of SPADE for moment estimation, note that, in the subdiffraction regime, Eq. (13) can be expressed as $\Theta_{\boldsymbol{\mu}} = \theta_{\boldsymbol{\mu}} + O(\Delta^{|\boldsymbol{\mu}|_1+2})$, where $O(\Delta^{|\boldsymbol{\mu}|_1+2})$ is a linear combination of moments that are at least two orders above $\boldsymbol{\mu}$. Moreover, assume for simplicity that each \mathbf{q} th channel in the TEM scheme is used to estimate only $\theta_{2\mathbf{q}}$ and not the higher-order moments, and the effect of $O(\Delta^{|\boldsymbol{\mu}|_1+2})$ nuisance parameters is negligible. The relevant Fisher information, given Eq. (15), becomes

$$J_{\boldsymbol{\mu}\boldsymbol{\mu}}^{(\text{TEM})}(\theta) = N^{(\text{TEM})} \frac{C(\mathbf{q}, \mathbf{q})}{\Theta_{2\mathbf{q}}}, \quad \boldsymbol{\mu} = 2\mathbf{q}, \quad (25)$$

where $N^{(\text{TEM})}$ is the average photon number available to the TEM scheme. A precision enhancement factor can be defined as the ratio of Eq. (25) to the corresponding component of Eq. (24), viz.,

$$\frac{J_{\boldsymbol{\mu}\boldsymbol{\mu}}^{(\text{TEM})}}{J_{\boldsymbol{\mu}\boldsymbol{\mu}}^{(\text{direct})}} \approx \frac{N^{(\text{TEM})}}{N} \frac{\boldsymbol{\mu}!}{2^{|\boldsymbol{\mu}|_1} (\boldsymbol{\mu}/2)! \Theta_{\boldsymbol{\mu}}} \quad (26)$$

to the leading order of Δ . Apart from a factor $N^{(\text{TEM})}/N$ determined by the different photon numbers detectable in each

method, the important point is that the factor scales inversely with

$$\Theta_{\boldsymbol{\mu}} \leq \theta_{\boldsymbol{\mu}} \leq \left(\frac{\Delta}{2}\right)^{|\boldsymbol{\mu}|_1}, \quad (27)$$

so the enhancement is enormous in the $\Delta \ll 1$ subdiffraction regime. The prefactor in Eq. (26) also increases with increasing $\boldsymbol{\mu}$.

For the other moments, assume that each iTEM measurement of the $(\mathbf{q}, \mathbf{q}')$ channels is used to estimate $\theta_{\mathbf{q}+\mathbf{q}'}$ only. It can then be shown using Eqs. (17) that the information is lower-bounded as

$$J_{\boldsymbol{\mu}\boldsymbol{\mu}}^{(\text{iTEM})}(\theta) \geq N^{(\text{iTEM})} \frac{2C^2(\mathbf{q}, \mathbf{q}')}{\beta(\mathbf{q}, \mathbf{q}')}, \quad \boldsymbol{\mu} = \mathbf{q} + \mathbf{q}', \quad (28)$$

where $N^{(\text{iTEM})}$ is the average photon number available to the iTEM scheme. An enhancement factor can be expressed as

$$\frac{J_{\boldsymbol{\mu}\boldsymbol{\mu}}^{(\text{iTEM})}}{J_{\boldsymbol{\mu}\boldsymbol{\mu}}^{(\text{direct})}} \approx \frac{N^{(\text{iTEM})}}{N} \frac{\boldsymbol{\mu}!}{2^{2|\boldsymbol{\mu}|_1-1} \mathbf{q}! (\boldsymbol{\mu} - \mathbf{q})! \beta(\mathbf{q}, \boldsymbol{\mu} - \mathbf{q})}, \quad (29)$$

With the background parameter $\beta(\mathbf{q}, \boldsymbol{\mu} - \mathbf{q})$ on the order of $\Delta^{\min[2\mathbf{q}_1, 2(\boldsymbol{\mu} - \mathbf{q})_1]}$, both $1/\beta$ and the $\boldsymbol{\mu}!/[q!(\boldsymbol{\mu} - \mathbf{q})!]$ coefficient can be maximized by choosing \mathbf{q} to be as close to $\boldsymbol{\mu}/2$ as possible. This justifies the pairing of neighboring modes in the iTEM schemes listed in Fig. 1 and Table I. With iTEM1, iTEM2, iTEM4, and iTEM5, $|\boldsymbol{\mu}|_1$ is odd, and

$$\beta = O(\Delta^{|\boldsymbol{\mu}|_1-1}). \quad (30)$$

With iTEM3 and iTEM6, $|\boldsymbol{\mu}|_1$ is even, and

$$\beta = O(\Delta^{|\boldsymbol{\mu}|_1}). \quad (31)$$

The enhancements, inversely proportional to β , can again be substantial for higher moments. The only exception is the estimation of the first moments θ_{10} and θ_{01} , for which the right-hand side of Eq. (29) becomes $N^{(\text{iTEM})}/N$ and the iTEM schemes offer no advantage.

These results can be compared with Refs. [1, 6] for the special case of two equally bright point sources. If the origin of the image plane is aligned with their centroid and their separation along the X direction is d , $\theta_{20} = d^2/4$, and a reparameterization leads to a transformed Fisher information $\mathcal{J}^{(\text{direct})}(d) \approx Nd^2/8$ and $\mathcal{J}^{(\text{TEM})}(d) \approx N/4$ for the estimation of d , in accordance with the results in Refs. [1, 6] to the leading order of d . The experiments reported in Refs. [12–14] serve as demonstrations of the proposed scheme in this special case.

C. Elementary explanation

The enhancements offered by SPADE can be understood by considering the signal-to-noise ratio (SNR) of a measurement with Poisson statistics. Suppose for simplicity that the mean count of an output can be written as $Np(j|\theta) = A\theta + B$,

which consists of a signal component $A\theta$ and a background B . The variance is $A\theta + B$, so the SNR can be expressed as $(A\theta)^2/(A\theta + B)$. To maximize it, the background B should be minimized to reduce the variance. For direct imaging, the background according to Eq. (19) is dominated by the TEM₀₀ mode, whereas each output of SPADE is able to filter out that mode as well as other irrelevant low-order modes to minimize the background without compromising the signal. To wit, Eq. (15) for TEM measurements has no background (assuming $\Theta_\mu \approx \theta_\mu$), while Eqs. (17) for iTEM also have low backgrounds in the subdiffraction regime. The Fisher information given by Eq. (6) is simply a more rigorous statistical tool that formalizes the SNR concept and provides error bounds; reducing the background likewise improves the information by reducing the denominator in Eq. (6).

In this respect, the proposed scheme seems to work in a similar way to nulling interferometry for exoplanet detection [50]. The nulling was proposed there for the special purpose of blocking the glare of starlight, however, and there had not been any prior statistical study of nulling for subdiffraction objects to my knowledge. The surprise here is that coherent processing in the far field can vastly improve general incoherent imaging even in the subdiffraction regime and in the presence of photon shot noise, without the need to manipulate the sources as in prior superresolution microscopic methods [51–56] or detect evanescent waves via lossy or unrealistic materials [57, 58].

V. NUMERICAL DEMONSTRATION

Here I present a numerical study to illustrate the proposal and confirm the theory. Assume an object that consists of 5 equally bright point sources with random positions within the square $-0.3 \leq X \leq 0.3$ and $-0.3 \leq Y \leq 0.3$. The average photon number is assumed to be $N = 5 \times 10,000$ in total. Figure 2 shows an example of the generated source positions and a direct image with pixel size $\delta x \delta y = 0.1 \times 0.1$ and Poisson noise. I focus on the estimation of the first and second moments of the source distribution given by $\{\theta_\mu; \mu = (1, 0), (0, 1), (2, 0), (0, 2), (1, 1)\}$. For direct imaging, I use the estimator $\hat{\theta}_\mu = \mu! \sum_j D_\mu(\mathbf{r}_j) m(\mathbf{r}_j) / N$, where $m(\mathbf{r}_j)$ is the photon count at a pixel positioned at \mathbf{r}_j . It can be shown that, in the small-pixel limit, this estimator is unbiased and approaches the CRB determined by Eq. (24) for $\Delta \ll 1$.

For SPADE, I consider only the TEM₀₀, TEM₁₀, and TEM₀₁ modes, and the photons in all the other modes are discarded. As illustrated in Fig. 3, the iTEM1, iTEM2, and iTEM3 schemes suffice to estimate the parameters of interest. Table II lists the projections, and Fig. 4 plots the spatial wave functions for the projections. The light is assumed to be split equally among the three schemes, leading to 9 outputs; Fig. 5 shows a sample of the photon counts drawn from Poisson statistics. Compared with the large number of pixels in direct imaging, the compressive nature of SPADE for moment estimation is an additional advantage.

Defining m_{jk} as the matrix of the photon counts of the 9 outputs in the order of Table II and Fig. 4, I assume an estima-

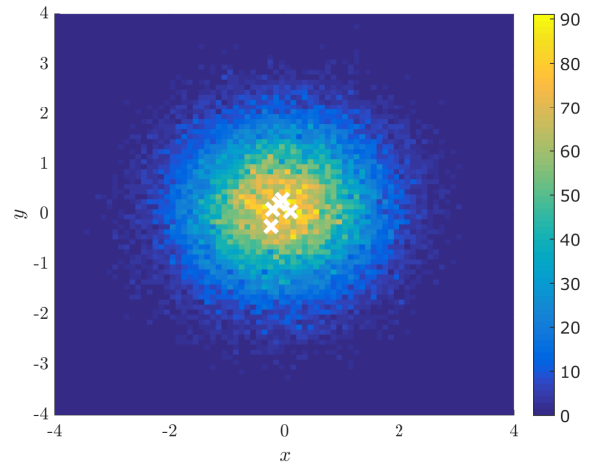


FIG. 2. The white crosses denote the 5 randomly generated source positions. The background image is a direct image with pixel size $\delta x \delta y = 0.1 \times 0.1$ (normalized with respect to the PSF width) and Poisson noise; the average photon number is $N = 5 \times 10,000$ in total.

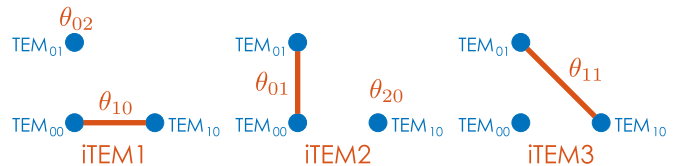


FIG. 3. A graphical representation of the iTEM1, iTEM2, and iTEM3 schemes involving the three TEM modes to be measured. Each line denotes an interferometer between two modes, and each unconnected dot denotes a TEM mode to be measured. The modes are also denoted by the parameters θ_μ to which they are sensitive.

iTEM1	iTEM2	iTEM3
$(00\rangle + 10\rangle)/\sqrt{2}$	$(00\rangle + 01\rangle)/\sqrt{2}$	$(10\rangle + 01\rangle)/\sqrt{2}$
$(00\rangle - 10\rangle)/\sqrt{2}$	$(00\rangle - 01\rangle)/\sqrt{2}$	$(10\rangle - 01\rangle)/\sqrt{2}$
$ 01\rangle$	$ 10\rangle$	$ 00\rangle$

TABLE II. The projections for the SPADE measurement scheme depicted in Fig. 3. $|00\rangle$ corresponds to the TEM₀₀ mode, $|10\rangle$ corresponds to the TEM₁₀ mode, and $|01\rangle$ corresponds to the TEM₀₁ mode.

tor given by $\check{\theta}_{10} = 3(m_{11} - m_{21})/N$, $\check{\theta}_{01} = 3(m_{12} - m_{22})/N$, $\check{\theta}_{20} = 12m_{32}/N$, $\check{\theta}_{02} = 12m_{31}/N$, and $\check{\theta}_{11} = 6(m_{13} - m_{23})/N$. This linear estimator comes from a straightforward inversion of Eqs. (15) and (17), assuming $\Theta_\mu = \theta_\mu$ and an average of $N/3$ photons available to each scheme. The iTEM background $m_{13} + m_{23}$ contains more information about $\theta_{20} + \theta_{02}$ that can be used in a more complicated estimator to lower the errors further, but the simple estimator here suffices for the demonstration.

Figure 6 plots the numerically computed mean-square errors (MSEs) for 100 randomly generated objects versus true parameters in log-log scale. Each error value for a given object is computed by averaging the squared difference between

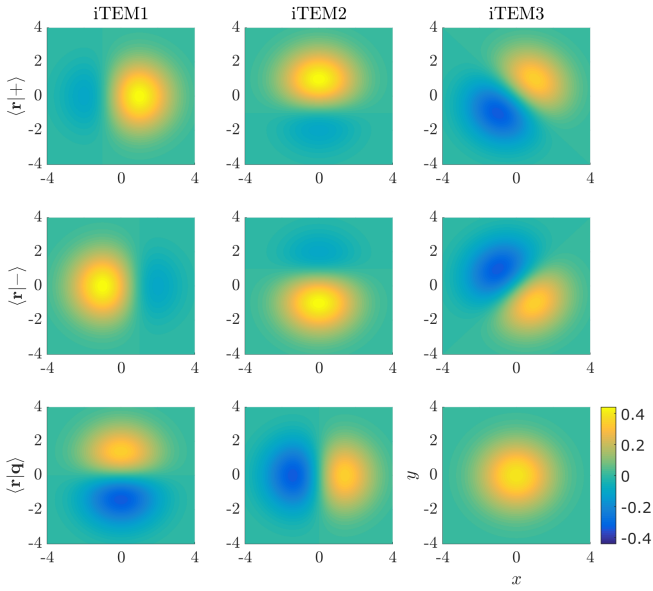


FIG. 4. The spatial wave functions $\langle \mathbf{r} | \phi_j \rangle$ for the projections listed in Table II. x and y are image-plane coordinates normalized with respect to the PSF width and the color code corresponds to amplitudes of normalized wave functions.

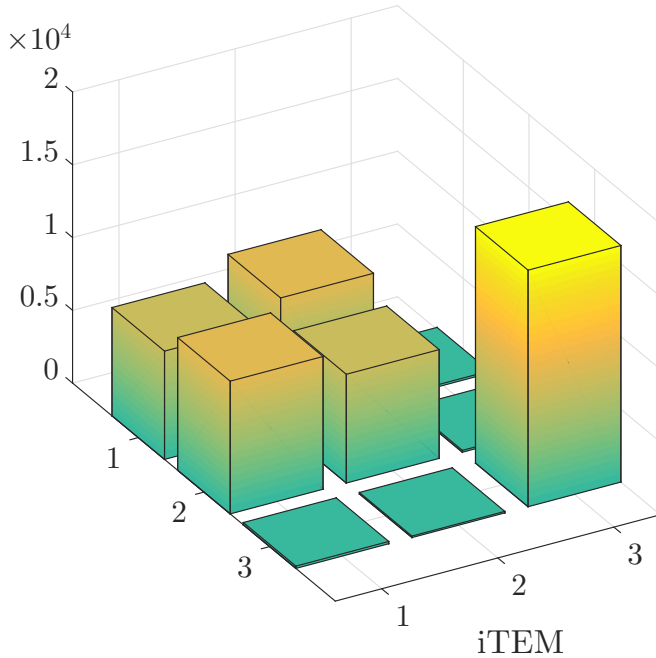


FIG. 5. A sample of the simulated photon counts from SPADE. The order of the matrix elements follows Table II and Fig. 4. Note how the counts for the antisymmetric modes are much lower as a result of filtering out the lower-order modes. As argued in Sec. IVIV C, such dark ports enable a higher SNR by reducing the background without compromising the signal.

the estimator and the true parameter over 500 samples of Poissonian outputs. For comparison, Fig. 6 also plots the CRBs given by the inverse of Eqs. (24), (25), and (28), assuming $\Theta_\mu = \theta_\mu$ and neglecting the $O(\Delta)$ term in Eq. (24). A few observations can be made:

1. As shown by the plots in the first row of Fig. 6, SPADE is 3 times worse than direct imaging at estimating the first moments. This is because SPADE uses only 1/3 of the available photons to estimate each first moment.
2. The other plots show that SPADE is substantially more precise at estimating the second moments, even though SPADE uses only a fraction of the available photons to estimate each moment. This enhancement is a generalization of the recent results on two sources [1–6, 8, 9, 11–14].
3. The errors are all remarkably tight to the CRBs, despite the simplicity of the estimators and the approximations in the bounds. In particular, the excellent performance of the SPADE estimator in the subdiffraction regime justifies its negligence of the difference between Θ_μ and θ_μ .

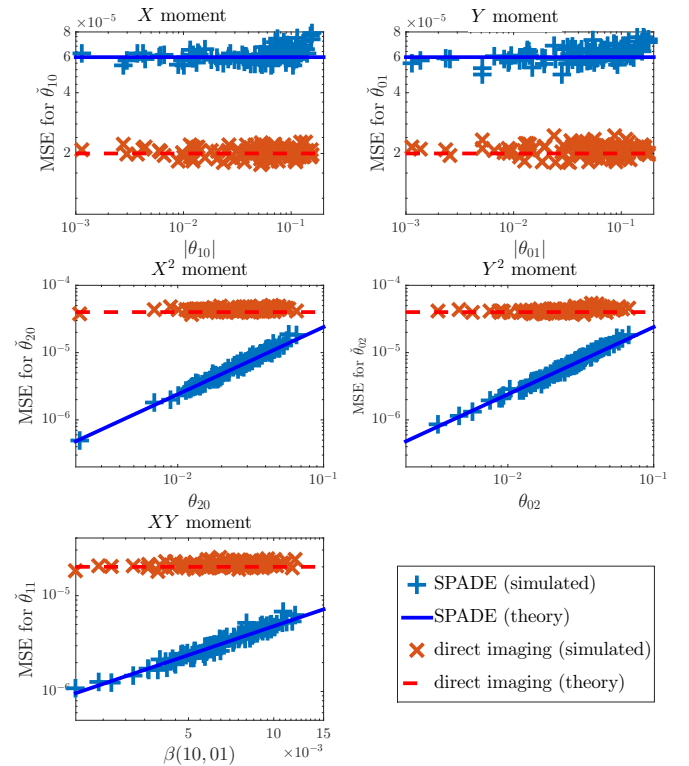


FIG. 6. Simulated errors for SPADE and direct imaging versus certain parameters of interest in log-log scale. The lines are the CRBs given by the inverse of Eqs. (24), (25), and (28), assuming $\Theta_\mu = \theta_\mu$ and neglecting the $O(\Delta)$ term in Eq. (24). Recall that all lengths are normalized with respect to the PSF width σ , so the first moments θ_{10} and θ_{01} are in units of σ , their MSEs are in units of σ^2 , the second moments θ_{20} , θ_{02} , θ_{11} , $\beta(10,01) = (\theta_{20} + \theta_{02})/8$ are in units of σ^2 , and their MSEs are in units of σ^4 .

VI. DISCUSSION

Though promising, the giant precision enhancements offered by SPADE do not imply unlimited imaging resolution for finite photon numbers. The higher moments are still more difficult to estimate even with SPADE in terms of the fractional error, which is $\sim 1/(\theta_\mu^2 J_{\mu\mu}) = 1/O(N\Delta^{|\mu|_1})$ for even $|\mu|_1$ and $1/O(N\Delta^{|\mu|_1+1})$ for odd $|\mu|_1$, meaning that more photons are needed to attain a desirable fractional error for higher $|\mu|_1$. Intuitively, this is because of the inherent inefficiency of subdiffraction objects to couple to higher-order modes, and the need to accumulate enough photons in those modes to achieve an acceptable SNR. A related issue is the reconstruction of the full source distribution, which requires all moments in principle. A finite number of moments cannot determine the distribution uniquely by themselves [42], although a wide range of regularization methods, such as maximum entropy and basis pursuit, are available for more specific scenarios [42, 46, 48, 59, 60].

Despite these limitations, the fact remains that direct imaging is an even poorer choice of measurement for subdiffraction objects and SPADE can extract much more information, simply from the far field. For example, the size and shape of a star, a planetary system, a galaxy, or a fluorophore cluster that is poorly resolved under direct imaging can be identified much more accurately through the estimation of the second or higher moments by SPADE. Alternatively, SPADE can be used to reach a desirable precision with far fewer photons or a much smaller aperture, enhancing the speed or reduc-

ing the size of the imaging system. In view of the results in Refs. [2, 4, 6], the image-inversion interferometers proposed in Refs. [2, 4, 6, 22–24] are expected to be similarly useful for estimating the second moments. For larger objects, scanning in the manner of confocal microscopy [26] or adaptive alignment [1] should be helpful.

Many open problems remain; chief among them are the incorporation of prior information, generalizations for non-Gaussian PSFs, the derivation of fundamental quantum limits, the possibility of even better measurements, and experimental implementations. These are daunting problems, but may be attacked by more advanced methods in quantum metrology [61–64], quantum state tomography [65–67], compressed sensing [46–48, 67], and photonics design [43–45].

FUNDING INFORMATION

National Research Foundation, Singapore (NRF-NRFF2011-07); Ministry of Education, Singapore (R-263-000-C06-112).

ACKNOWLEDGMENTS

Inspiring discussions with Ranjith Nair, Xiao-Ming Lu, Shan Zheng Ang, Shilin Ng, Laura Waller’s group, Geoff Schiebinger, Ben Recht, and Alex Lvovsky are gratefully acknowledged.

-
- [1] M. Tsang, R. Nair, and X.-M. Lu, *Physical Review X* **6**, 031033 (2016).
 - [2] R. Nair and M. Tsang, *Optics Express* **24**, 3684 (2016).
 - [3] M. Tsang, R. Nair, and X.-M. Lu, in *Proc. SPIE*, Quantum and Nonlinear Optics IV, Vol. 10029 (2016) p. 1002903.
 - [4] R. Nair and M. Tsang, *Physical Review Letters* **117**, 190801 (2016).
 - [5] M. Tsang, [arXiv:1605.03799](https://arxiv.org/abs/1605.03799) [physics, physics:quant-ph] (2016).
 - [6] S. Z. Ang, R. Nair, and M. Tsang, [arXiv:1606.00603](https://arxiv.org/abs/1606.00603) [physics, physics:quant-ph] (2016).
 - [7] X.-M. Lu, R. Nair, and M. Tsang, [arXiv:1609.03025](https://arxiv.org/abs/1609.03025) [quant-ph] (2016).
 - [8] C. Lupo and S. Pirandola, *Physical Review Letters* **117**, 190802 (2016).
 - [9] J. Rehacek, M. Paur, B. Stoklasa, L. Motka, Z. Hradil, and L. L. Sanchez-Soto, [arXiv:1607.05837](https://arxiv.org/abs/1607.05837) [quant-ph] (2016).
 - [10] H. Krovi, S. Guha, and J. H. Shapiro, [arXiv:1609.00684](https://arxiv.org/abs/1609.00684) [physics, physics:quant-ph] (2016).
 - [11] Z. S. Tang, K. Durak, and A. Ling, *Optics Express* **24**, 22004 (2016).
 - [12] F. Yang, A. Tashchilina, E. S. Moiseev, C. Simon, and A. I. Lvovsky, *Optica* **3**, 1148 (2016).
 - [13] W. K. Tham, H. Ferretti, and A. M. Steinberg, [arXiv:1606.02666](https://arxiv.org/abs/1606.02666) [physics, physics:quant-ph] (2016), accepted by *Physical Review Letters*.
 - [14] M. Paúr, B. Stoklasa, Z. Hradil, L. L. Sánchez-Soto, and J. Rehacek, *Optica* **3**, 1144 (2016).
 - [15] E. Bettens, D. Van Dyck, A. J. den Dekker, J. Sijbers, and A. van den Bos, *Ultramicroscopy* **77**, 37 (1999).
 - [16] S. Van Aert, A. J. den Dekker, D. Van Dyck, and A. van den Bos, *Journal of Structural Biology* **138**, 21 (2002).
 - [17] S. Ram, E. S. Ward, and R. J. Ober, *Proceedings of the National Academy of Sciences of the United States of America* **103**, 4457 (2006).
 - [18] C. O. Acuna and J. Horowitz, *Journal of Applied Statistics* **24**, 421 (1997).
 - [19] J. G. Walker, G. J. Brakenhoff, M. Bertero, E. R. Pike, R. E. Davies, and M. R. Young, *J. Opt. Soc. Am. A* **10**, 59 (1993).
 - [20] F. Tamburini, G. Anzolin, G. Umbriaco, A. Bianchini, and C. Barbieri, *Physical Review Letters* **97**, 163903 (2006).
 - [21] N. Sandeau and H. Giovannini, *Journal of the Optical Society of America A* **23**, 1089 (2006).
 - [22] K. Wicker and R. Heintzmann, *Optics Express* **15**, 12206 (2007).
 - [23] K. Wicker, S. Sindbert, and R. Heintzmann, *Optics Express* **17**, 15491 (2009).
 - [24] D. Weigel, R. Foerster, H. Babovsky, A. Kiessling, and R. Kowarschik, *Optics Express* **19**, 26451 (2011).
 - [25] R. J. Prokop and A. P. Reeves, *CVGIP: Graphical Models and Image Processing* **54**, 438 (1992).
 - [26] J. B. Pawley, ed., *Handbook of Biological Confocal Microscopy* (Springer, New York, 2006).

- [27] H. Deschout, F. C. Zanacchi, M. Mlodzianoski, A. Diaspro, J. Bewersdorf, S. T. Hess, and K. Braeckmans, *Nature Methods* **11**, 253 (2014).
- [28] K. I. Mortensen, L. S. Churchman, J. A. Spudich, and H. Flyvbjerg, *Nature Methods* **7**, 377 (2010).
- [29] J. Chao, E. Sally Ward, and R. J. Ober, *Journal of the Optical Society of America A* **33**, B36 (2016).
- [30] M. C. E. Huber, A. Pauluhn, J. L. Culhane, J. G. Timothy, K. Wilhelm, and A. Zehnder, eds., *Observing Photons in Space: A Guide to Experimental Space Astronomy* (Springer, New York, 2013).
- [31] R. Davies *et al.*, in *Proc. SPIE*, Ground-based and Airborne Instrumentation for Astronomy VI, Vol. 9908 (2016) p. 99081Z.
- [32] J. Zmuidzinas, *J. Opt. Soc. Am. A* **20**, 218 (2003).
- [33] J. W. Goodman, *Statistical Optics* (Wiley, New York, 1985).
- [34] J. W. Goodman, *Introduction to Fourier Optics* (McGraw-Hill, New York, 2004).
- [35] J. H. Shapiro, *IEEE Journal of Selected Topics in Quantum Electronics* **15**, 1547 (2009).
- [36] L. A. Wasserman, *All of Statistics* (Springer, New York, 2004).
- [37] H. L. Van Trees, *Detection, Estimation, and Modulation Theory, Part I* (John Wiley & Sons, New York, 2001).
- [38] A. Yariv, *Quantum Electronics* (Wiley, New York, 1989).
- [39] DLMF, “NIST Digital Library of Mathematical Functions,” <http://dlmf.nist.gov/>, Release 1.0.11 of 2016-06-08, online companion to [40].
- [40] F. W. J. Olver, D. W. Lozier, R. F. Boisvert, and C. W. Clark, eds., *NIST Handbook of Mathematical Functions* (Cambridge University Press, New York, NY, 2010) print companion to [39].
- [41] L. Mandel and E. Wolf, *Optical Coherence and Quantum Optics* (Cambridge University Press, Cambridge, 1995).
- [42] M. Bertero, in *Advances in Electronics and Electron Physics*, Vol. 75, edited by P. W. Hawkes (Academic Press, 1989) pp. 1–120.
- [43] S. Armstrong, J.-F. Morizur, J. Janousek, B. Hage, N. Treps, P. K. Lam, and H.-A. Bachor, *Nature Commun.* **3**, 1026 (2012).
- [44] D. A. B. Miller, *Photonics Research* **1**, 1 (2013).
- [45] G. Li, N. Bai, N. Zhao, and C. Xia, *Advances in Optics and Photonics* **6**, 413 (2014).
- [46] Y. de Castro and F. Gamboa, *Journal of Mathematical Analysis and Applications* **395**, 336 (2012).
- [47] E. J. Candès and C. Fernandez-Granda, *Communications on Pure and Applied Mathematics* **67**, 906 (2014).
- [48] G. Schiebinger, E. Robeva, and B. Recht, [arXiv:1506.03144 \[cs, math\]](https://arxiv.org/abs/1506.03144) (2015).
- [49] D. R. Cox and N. Reid, *Journal of the Royal Statistical Society. Series B (Methodological)* **49**, 1 (1987).
- [50] A. Labeyrie, S. G. Lipson, and P. Nisenson, *An Introduction to Optical Stellar Interferometry* (Cambridge University Press, Cambridge, 2006).
- [51] W. E. Moerner, *Proceedings of the National Academy of Sciences* **104**, 12596 (2007).
- [52] E. Betzig, G. H. Patterson, R. Sougrat, O. W. Lindwasser, S. Olenych, J. S. Bonifacino, M. W. Davidson, J. Lippincott-Schwartz, and H. F. Hess, *Science* **313**, 1642 (2006).
- [53] S. W. Hell, *Science* **316**, 1153 (2007).
- [54] M. I. Kolobov, ed., *Quantum Imaging* (Springer, New York, 2007).
- [55] M. A. Taylor, J. Janousek, V. Daria, J. Knittel, B. Hage, H.-A. Bachor, and W. P. Bowen, *Nature Photonics* **7**, 229 (2013).
- [56] M. Tsang, *Optica* **2**, 646 (2015).
- [57] J. B. Pendry, *Physical Review Letters* **85**, 3966 (2000).
- [58] M. Tsang and D. Psaltis, *Physical Review B* **77**, 035122 (2008).
- [59] S. F. Gull and J. Skilling, *IEEE Proceedings F - Communications, Radar and Signal Processing* **131**, 646 (1984).
- [60] P. Milanfar, W. C. Karl, and A. S. Willsky, *IEEE Transactions on Image Processing* **5**, 459 (1996).
- [61] M. Hayashi, *Quantum Information* (Springer, Berlin, 2006).
- [62] J. Kahn and M. Guță, *Communications in Mathematical Physics* **289**, 597 (2009).
- [63] D. W. Berry, M. Tsang, M. J. W. Hall, and H. M. Wiseman, *Phys. Rev. X* **5**, 031018 (2015).
- [64] X.-M. Lu and M. Tsang, *Quantum Science and Technology* **1**, 015002 (2016).
- [65] M. Ježek and Z. Hradil, *Journal of the Optical Society of America A* **21**, 1407 (2004).
- [66] A. I. Lvovsky and M. G. Raymer, *Reviews of Modern Physics* **81**, 299 (2009).
- [67] D. Gross, Y.-K. Liu, S. T. Flammia, S. Becker, and J. Eisert, *Phys. Rev. Lett.* **105**, 150401 (2010).